International Journal of Engineering, Mathematical and Physical Sciences
ISSN: 2517-9934
Vol:13, No:4, 2019

Multiphase Flow Regime Detection Algorithm for Gas-Liquid Interface Using Ultrasonic Pulse-Echo Technique

Serkan Solmaz, Jean-Baptiste Gouriet, Nicolas Van de Wyer, Christophe Schram

***Abstract*—**Efficiency of the cooling process for cryogenic propellant boiling in engine cooling channels on space applications is relentlessly affected by the phase change occurs during the boiling. The effectiveness of the cooling process strongly pertains to the type of the boiling regime such as nucleate and film. Geometric constraints like a non-transparent cooling channel unable to use any of visualization methods. The ultrasonic (US) technique as a non-destructive method (NDT) has therefore been applied almost in every engineering field for different purposes. Basically, the discontinuities emerge between mediums like boundaries among different phases. The sound wave emitted by the US transducer is both transmitted and reflected through a gas-liquid interface which makes able to detect different phases. Due to the thermal and structural concerns, it is impractical to sustain a direct contact between the US transducer and working fluid. Hence the transducer should be located outside of the cooling channel which results in additional interfaces and creates ambiguities on the applicability of the present method. In this work, an exploratory research is prompted so as to determine detection ability and applicability of the US technique on the cryogenic boiling process for a cooling cycle where the US transducer is taken place outside of the channel. Boiling of the cryogenics is a complex phenomenon which mainly brings several hindrances for experimental protocol because of thermal properties. Thus substitute materials are purposefully selected based on such parameters to simplify experiments. Aside from that, nucleate and film boiling regimes emerging during the boiling process are simply simulated using non-deformable stainless steel balls, air-bubble injection apparatuses and air clearances instead of conducting a real-time boiling process. A versatile detection algorithm is perennially developed concerning exploratory studies afterward. According to the algorithm developed, the phases can be distinguished 99% as no-phase, air-bubble, and air-film presences. The results show the detection ability and applicability of the US technique for an exploratory purpose.

***Keywords*—**Ultrasound, ultrasonic, multiphase flow, boiling, cryogenics, detection algorithm.

I. Introduction

THE US assessment as an NDT is a common application used without causing any damage to the systems whereas nontransparent structures are present. It is an appropriate tool to detect irregular structures inside homogeneous domains such as multiphase flows. Sound waves with frequencies above 20 kHz, the upper limit of human hearing, might be called either Ultrasonic or Ultrasound. In most common US devices transmit a center-frequency ranging from 0.1 to 15 MHz in order to detect non-homogeneous structures [1]. Simple description of US technique belongs to sound pressure wave propagation inside mediums which transports mechanical energy generated by US probe throughout the local vibration of particles at frequencies higher than 20 kHz. The US wave is continuously transmitted in the homogeneous medium until reaching an irregular structure which results in reflection of the wave on the reverse direction, thereby providing an outcome for detection as illustrated in Fig. 1. Furthermore, although the energy released by the US probe is intensive, it is usually lower than 1 W/cm^2 that cannot alter both the physical and chemical properties of the materials examined. Hence the US technique may be considered an NDT method [2].

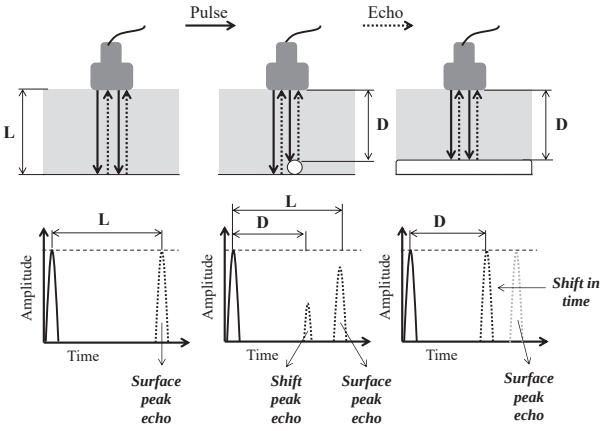

(a) Single phase (b) Bubble (c) Film

Fig. 1 Propagation of the US waves and simplified echogram for the different cases; (a) single phase; (b) water & air-bubble; (c) water & air-film

Phase change in the fluid flow due to heat transfer during both heating and cooling processes had been broadly investigated as an exploratory topic by researchers in order to understand, improve, and optimize thermal systems. Essentially, fluid flow in boiling regime is extremely affected by the phase change which emerges in regards to the temperature difference between working fluid and heated surface. Several journal articles have been found achieving detection of the liquid & bubble interface, the bubble void

S. Solmaz is with the Environmental and Applied Fluid Dynamics Department, von Karman Institute for Fluid Dynamics, Waterloosesteenweg 72, B-1640 Sint-Genesius-Rode, Belgium (phone: +32486134874; e-mail: serknslmz@gmail.com).

J.-B. Gouriet, N. Van de Wyer, and C. Schram are with the Environmental and Applied Fluid Dynamics Department, von Karman Institute for Fluid Dynamics, Waterloosesteenweg 72, B-1640 Sint-Genesius-Rode, Belgium (e-mail: gouriet@vki.ac.be, nicolas.vandewyer@vki.ac.be, christophe.schram@vki.ac.be).

fraction, flow properties, and appropriate post-processing method. The bubble diameters inspected in these studies differ between 0.5 to 12 mm belong to conditions where the US frequencies vary 1 to 15 MHz. A study had been conducted determining single argon bubbles diameter rising in distilled water and 7% difference between the US technique and high speed camera visualization had been obtained [3]. According to study carried out by [4] in order to figure out the velocity profile of air bubble inside the water, 6% difference had been declared between the US techniques and PIV test. Reference [5] prompted an experimental study to detect the interface considering 2.5 to 5 mm air bubbles injected into water, and hereby 99% of accuracy had been declared. Having examined studies applied the US technique for detecting bubble related parameters, it can therefore be concluded that the US technique is an appropriate method for the present study as well. In addition, no article has been found on literature proposing an unique algorithm to distinguish different regimes like no-phase, nucleate and film for a mere case based on the boiling flow.

In this exploratory study, the ultimate motivation is to determine detection ability and applicability of the US techniques so as to develop an appropriate detection algorithm which practically distinguishes phases. Initially, the detection ability of the US technique is assessed using a preliminary setup in which the US transducer is directly immersed in working fluid. However, the US transducer should be placed outside of the cooling channel for real application due to thermal and geometric constraints. This arrangement adversely affects the pulse-echo propagation whereas several interfaces emerge between the US transducer and target point. A secondary setup is subsequently designed to explore the applicability of the US technique concerning geometric constraints for the real application. Fig. 2 illustrates the fundamental difference between preliminary and secondary setups in terms of pulse-echo propagation through interfaces.

As the complex nature of the boiling process and cryogenics which bring several hurdles to experimental protocol, substitute materials are therefore taken into account in order to simplify the present study thoroughly. Likewise, nucleate and film boiling regimes emerging during the boiling process are basically simulated using air-bubble injection apparatuses and air clearances instead of conducting a real-time boiling. Experimental results show that phases can easily be distinguished by the US technique due to certain aspects obtained from echograms. Following all those outcomes acquired from experiments, a detection algorithm is eventually developed which detects different phases as no-phase, bubble, and film within an accuracy of 99%.

II. Materials and Methods

A. Pulse-Echo Method

Sound waves released by the transducer propagate inside the domain from one point to another without transfer of matter. For the pulse-echo method, the sound wave has a longitudinal characteristic in which the wave motion is aligned with the wave direction and propagates by adiabatic compression and decompression. A piezoelectric US transducer has dual functions transmitting wave (pulse) into the domain and receiving reflected ones (echo) to detect any of substances. For homogeneous mediums, the wave is transmitted inside the domain without any loses theoretically until reaching a certain region where discontinuities are available because of interface among different substances. The sound waves are both transmitted and reflected in case an interface emerges on the path of propagation.

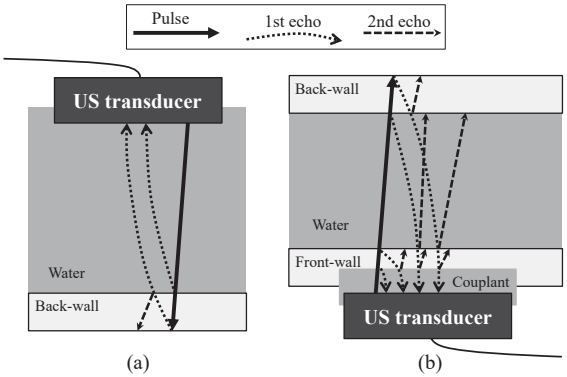

Fig. 2 Pulse-echo propagation through interfaces for different arrangements in which; (a) the US transducer is directly immersed into water; (b) the US transducer is taken place outside of the channel using couplant

The main property causing discontinuity between different mediums is characteristic acoustic impedance (Z) proportional to density (ρ) of the medium and speed of sound (c) inside the medium which can simply be calculated as Z_{medium}=ρ c. The closer acoustic impedances get for two mediums, the more transmitted the wave becomes. This phenomenon for the perfect transmission due to similar impedances is called impedance-match [1]. In the present study, since the characteristic acoustic impedances of the liquid and gas phases are quite different from each other, it results in a distinctive behavior through boundaries in terms of reflection.

Whilst a normal incidence wave reaches a region acoustically discontinuous, reflection at boundaries and transmission through the second medium are presented in accordance with acoustic impedances to sustain conservation of mass, momentum and energy. Reflection (R) coefficient defined based on the difference between characteristic acoustic impedances can be found with (1), where subscript 1 is the medium that normal incidence coming through, and subscript 2 is the medium that wave transmitted. The relationship between transmission and reflection is expressed with 1+R=T. In terms of energy intensity, the coefficient should be rearranged considering conservation of energy law in which R_e=R^2 and thereby 1=R_e+T_e [6].

$$R = \frac{Z_2 - Z_1}{Z_2 + Z_1} \tag{1}$$

Properties of acoustic wave are essential to define in advance to compare experimental study against theory, thereby ensuring validation of the applied method. The relationship between US frequency (f) and speed of sound (c) can be described by wavelength (λ) which emphasizes penetration

through a medium examined in (2). Yet the amplitude of US wave reduces through propagation, the frequency is kept constant.

$$\lambda = \frac{c}{f} \tag{2}$$

The distance between the US transducer and target surface can be estimated to compare against experimental study. The pulse emitted into domain propagates until the interface where acoustic impedance among mediums differs. Total duration between the pulse and the first reflection received by the transducer can be determined by (3) where d is the distance between the transducer and target surface, c is the speed of sound and t_{delay} is delay in duration until the first echo reaches to US transducer comprising round-trip of US wave.

$$d = \frac{c \times t_{delay}}{2} \tag{3}$$

The time interval between two adjacent emitted pulses is generally expressed with t_{total}. As a theoretical approach, t_{total} is determined by Pulse Repetition Frequency (PRF) which is the number of pulses repeating signal in a constant duration. In Fig. 3, US wave propagation including echogram is simply illustrated.

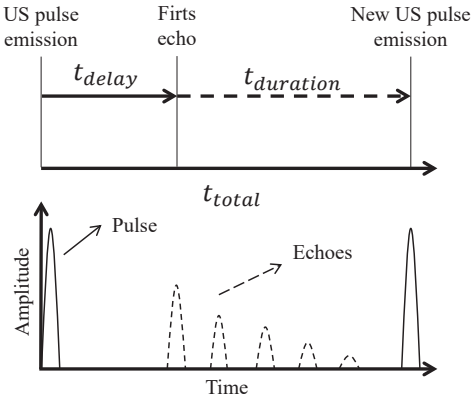

Fig. 3 A sample of time-scale for propagation of pulse and echoes using echogram

Moreover, the US beam structure is a significant parameter to bring the detection ability of the US technique into light. The incident US wave travels inside a homogeneous medium within a beam structure in which the intensity of the wave is attenuated gradually on the normal and radial direction. Intensity and characteristic of the US beam can be described by field distance, beam diameter, and central frequency [7]. A further method to extract the characteristic of a US beam is to generate isoecho contours for a certain cross-section underneath the US transducer, thereby describing detection ability for a local region.

B. Substitute Materials

The boiling temperature of cryogenics is very low compared to water at 1 ATM, and hence conducting an experimental study concerning cryogenics equire a huge amount of effort to sustain security, thermal conditions and so forth. The ultimate goal of the present study is intentionally distinguishing the phases emerge during the boiling process coarsely. Therefore thermal specifications of the corresponding fluids can simply be neglected.

Nucleate boiling is the most preferred regime due to increasing trend in heat flux rate that enables an efficient cooling & heating cycle within relatively low-temperature differences. Since phase change has a major effect on heat transfer characteristic of the boiling process, it is indeed a necessity to understand the rationale behind bubble formation and its effect on heat transfer. In nucleate boiling regime, bubble formation comprises there subsequent stages such as initialize, growth and detachment [8]. Likewise, it is substantial to express that increasing temperature difference causes covering the surface with vapor phase, thereby reducing heat flux.

Though the complex physical structure of cryogenics due to low operation temperatures causes a variation for the magnitude of temperature difference, phase change through boiling flow corresponds an almost identical tendency starting from bubble formation to film boiling. According to Randall and Gregory [8] a similar curve is obtainable for the boiling of cryogenics compared to pool boiling curve of the water. Apart from that, a thorough literature search has been carried out to pinpoint the bubble departure diameter for cryogenics and some other fluids as in Table I.

TABLE I
BUBBLE DEPARTURE DIAMETER OF SEVERAL FLUIDS FOR POOL BOILING CONDITIONS

Fluid	Bubble departure diameter (mm)
Water [9], [10]	1.5 - 2.5
Freon-12 [9]	0.7
CCl4 [9]	1.1
Ethanol [9]	1
Hydrogen [11]	1.5
Nitrogen [12], [13]	1 - 1.5
HFE-7000 [14], [15]	1

Characteristic acoustic impedance (Z) is a type of resistance that an ultrasound beam encounters as it passes through different mediums. It may evidently be interpreted that the high difference between the acoustic impedances of the gas (air) and liquid (water, HFE-7000, cryogenics, etc.) phases causes the reflection of almost 99% of incident wave. Hence the location of a gas-liquid interface can be determined with echogram by measuring the transit time between the pulse and first echo. Power reflection coefficients R^2 for several materials are expressed with Table II for ambient conditions.

HFE-7000 and water are the appropriate substitute fluids found in the literature in order to replace cryogenics based on the parameters that are bubble departure diameter, acoustic impedance, and boiling point. Since thermal properties are not taken into account for the present exploratory research, bubble departure diameter and acoustic impedance are the main parameters to consider. Besides, a special attention is paid using a non-deformable solid material in order to assess detection ability of US transducer within a preliminary study. Stainless steel ball might be considered a suitable

candidate to replace acoustic properties of cryogenics. Yet the non-deformable structure of materials is quite tedious to simulate bubble curvature, it is a robust method that gives an evidence on detection ability of US transducer to emphasize bubble departure diameter and distinguish sizes in a specific range. Minimum bubble departure diameter for cryogenics varies between 1 and 2 mm where nucleate boiling is the driven factor. Likewise, the power reflection coefficient for cryogenics varies between 0.9912 to 0.9978 that enables to use water and steel ball as substitute materials. To sum up, two experimental studies are designed using steel ball and air-bubble respectively.

C. Design of Experiments

Experimental study is purposefully divided into two main parts. The first case is to assess detection ability of the US technique using non-deformable stainless steel balls. Following these preliminary examinations, the applicability of the US technique is investigated by an experimental setup close to the real application in terms of geometric constraints. In order to simplify experimental protocol, the boiling process is simulated using non-deformable stainless steel balls for the first case and air injection apparatus for the second case.

1) Non-Deformable Body: A preliminary study is an asset to verify the detection ability of the US transducer to prevail over indecisive outcomes. Advantage of the preliminary research facility is to have a simple experimental procedure and a setup being easy to maintain. On the contrary, solid structure of non-deformable stainless steel ball and fully spherical curvature are the main compromises on bubble dynamics. Stainless steel balls with diameters 1 to 10 mm are examined to have a thorough investigation of the detection ability based on the bubble departure diameter for the nucleate boiling regime.

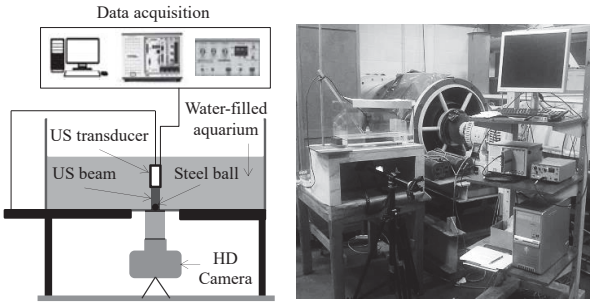

Fig. 4 Preliminary study using non-deformable facility setup to investigate detection ability of the US technique; (a) schematic of setup; (b) setup developed

Overview of the exploratory research facility is sketched in Fig. 4. A water-filled aquarium is used to plunge the US transducer to have a direct contact with working fluid. An immersion US transducer A309S-SU by Olympus implemented to the system is a single element longitudinal wave transducer. It is specifically designed to transmit ultrasound in applications whereas the test part is partially or wholly immersed. The transducer operating with 5 MHz central frequency has 13 mm nominal element size and 10 cm focal length. It is attached to the system within an aluminum holder arranged vertically.

A grid comprising several patterns is adhered below of the bottom surface of aquarium to ensure regional localization based on the pattern investigated as shown in Fig. 5. In order to track local displacement of the stainless steel ball underneath the transducer onto the grid, an HD portable camera Nikon COOLPIX P600 is fixed by a tripod. National Instruments PXIe-1073 chassis kit for data acquisition process and Olympus NDT Model 5077PR ultrasonic square wave pulser/receiver for US transducer are connected each other by a computer to combine all necessary equipment.

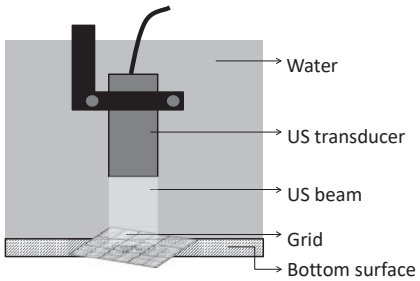

Fig. 5 Grid attached onto bottom surface of aquarium to locate stainless steel balls in regards to pattern examined

2) Air Injection: Following the preliminary experiments being conducted with non-deformable body facility, a secondary experimental facility is deliberately designed injecting air-bubble inside the water-filled tank. The main difference between preliminary and secondary experimental cases is illustrated in Fig. 13. Due to the geometric and thermal constraints, the US transducer should be taken place outside of the cooling channel which brings several ambiguities to explore.

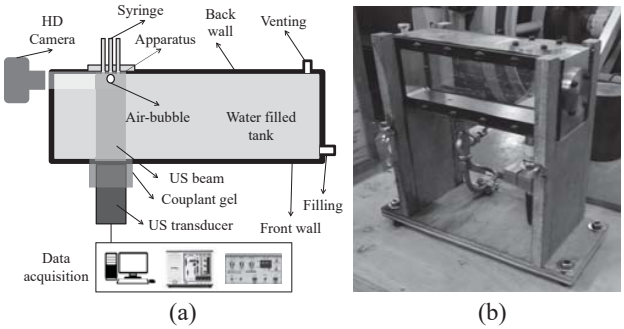

Fig. 6 Secondary study using bubble injection facility to investigate applicability of the US technique; (a) schematic of setup; (b) setup developed

Overview of the bubble injection facility is demonstrated in Fig. 6. Stainless steel apparatuses whereas the bubbles injected is intentionally preferred in accordance with the real application. The rectangular box filled with water is manufactured using aluminum. To enable visualization of

TABLE II
REFLECTION AND TRANSMISSION COEFFICIENTS FOR VARIOUS INTERFACES

Interface	Water to air (293 K)	Hydrogen to air (210 K)	Nitrogen to air (210 K)	HFE 7000 to air (293 K)	Water to glass	Water to aluminum	Water to plexiglass	Water to steel
R_e	0.9989	0.9912	0.9955	0.9978	0.6068	0.6973	0.1211	0.8741
T_e	0.0011	0.0088	0.0045	0.0022	0.3932	0.3027	0.8789	0.1259

injected bubble size using HD camera based on a reference object, side-walls are covered by transparent Plexiglas acrylic sheets. Hence the US measurements are compared against the HD camera to assess the applicability of the present technique. Venting and filling vanes are located to discharge and fill the impermeable box which is completely charged with water. The US transducer is sealed within the region which is polished 5 mm in deep to align transducer properly. The same types of equipment used in the preliminary setup are utilized for data acquisition.

Though the US transducer may directly be attached outside of the cooling channel without any hurdle, emitted pulses and received echoes are severely attenuated because of the air stuck between two contacting surfaces. The acoustic impedance of air is much lower compared to the surface material, and results in a substantial loss in transmission. In order to dope out this issue, the most common and affirmative method is using a US couplant which mitigates the effect of the wall occupied in front of the US transducer. In accordance with facilities including material, inspection angle, inspection volume and corrosion protection, a commercial Wavelength MP Ultrasound Acoustic Gel is used to implement between the transducer and the wall which is partially viscous and non-corrosive for metal surfaces.

Furthermore, in order to achieve the injection of air volume into water based on the bubble departure diameter in the nucleate regime, microliter syringes are implemented to apparatus generating bubbles with varying diameter 1 to 2 mm where total volumes are calculated 0.523 and 4.187 microliter, respectively. For this purpose Hamilton compatible Gastight High-Performance Microliter syringes with 1 and 5 microliter are obtained so as to inject air volume precisely. The needle gauge attached to syringe based on corresponding standards is 25 that connotes 0.26 mm inner diameter and 0.51 mm outer-diameter for the needle used. Likewise, a common milliliter syringe is applied for injection of diameters up to 7 mm.

III. RESULTS

The US technique is thoroughly investigated within partially simplified experimental cases based on substitute materials to determine applicability of the method detecting multiphase regimes. Subsequently, a detection algorithm is developed to run an automatic phase detection process for the flow encompassing different phases concurrently. Pulse repetition frequency (PRF), the number of pulses repeating signal in a constant duration, is set to 1 kHz which negates the interaction among adjacent pulses removing redundant echoes. Following the theory expressed for the pulse-echo and the US beam structure, the near field is calculated as 143 mm. The spread of the US beam is also determined 1 degree from centerline. The gain of signal acquired is adjusted for each experiment to increase the resolution of echoes received. Each measurement represents the average of 200 acquisitions, and uncertainty is calculated taking the number of samples 199 into account for estimator in order to refrain from bias.

A. Data Processing

The raw data should be scrutinized broadly which is a must to have a robust post-processing method directly affects outcomes of the study. A detection algorithm, driven by the raw data to specify either having an irregular structure inside the homogeneous medium, is developed afterward.

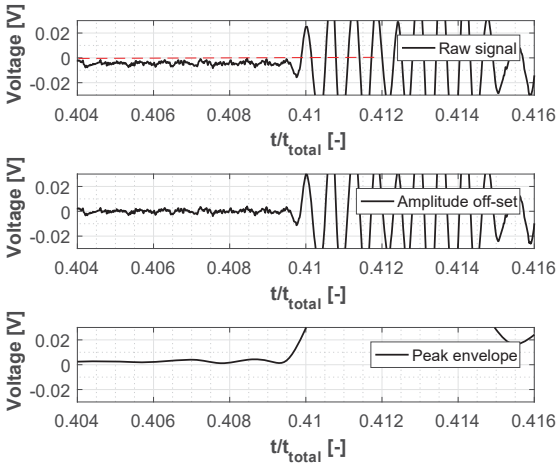

Fig. 7 A sample signal to figure out initial post-processing method following raw signal, amplitude off-set and peak generation

The signal has a trend on the negative side of echogram whilst no echoes are present. A correction is therefore needed to rectify the y-axis of signal around zero. To accomplish this, a deviation is calculated taking the average of signal whereas the acquired data merely belongs to system noise and is subsequently added to the whole signal.

The signal obtained from data acquisition has a rapidly oscillating characteristic due to pulse-echo propagation in an extremely short time order of microseconds. To create an envelope accompanying peak points, the raw signal should be transformed to an analytic signal implying the so-called Hilbert transform which has a real and phase-shifted complex version of the signal. In this study, the envelope is generated by using peak envelope function of Matlab 2016a which returns the upper envelopes of the input signal as the magnitude of its analytic signal.

Since signal characteristics of the results are hard to predict in advance, the post-processing method is also evaluated

throughout experiments conducted. A sample of the signal processed is expressed in detail by Fig. 7.

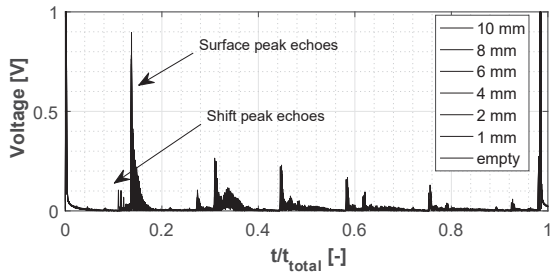

Fig. 8 A sample signal after post-processing for Pattern A comprising different ball diameters

B. Non-Deformable Body

A preliminary investigation using the non-deformable body facility has been carried out to explore detection ability of the US technique. The water temperature throughout experiments was measured 17 ° C. In Table III, experimental results and theoretical calculations are compared to obtain percentage differences for t_{delay} and $t_{duration}$ based on pulse-echo propagation. In terms of detection ability, 0.3 mm difference is determined between experimental results and theoretical calculations which is indeed acceptable concerning 1 mm bubble departure diameter for the nucleate boiling regime.

TABLE III
COMPARISON BETWEEN EXPERIMENTAL RESULT AND THEORETICAL CALCULATION BASED ON PULSE-ECHO PROPAGATION

Time domain (s)	Experiment	Theory	Difference (%)
t_delay	69.0	68.6	-0.591
t_duration	431.0	431.4	0.094
t_total	500.0	500.0	0

1) Pattern Investigation: An analysis has been prompted to investigate detection ability of the US technique using stainless steel balls with various diameters and local arrangements. In this study, stainless steel balls are taken place on the glass bottom surface underneath the US transducer. A grid comprising several patterns is adhered below the bottom surface of the aquarium to ensure distribution of the balls based on the pattern investigated. Diameter (Pattern A), location & distribution (Pattern B, C, D, and E) and overlapping (Pattern F) of the stainless steel balls are the cases explored experimentally using patterns shown in Fig. 9.

Fig. 8 illustrates the echogram obtained for Pattern A using single stainless steel balls of varying diameter. The echogram provides two unique characteristics so as to investigate detection ability of the US technique which are the shift and surface peak echoes. The magnitude and time delay for these echoes are the main parameters that provide to track changes. Results of pattern assessment can be concluded as follows.

Pattern A examines a single ball on the center of the grid for each diameter separately. Fig. 10 shows the change of shift peak echo properties for different ball diameters. Increasing diameter results in increasing magnitude of the shift peak echo

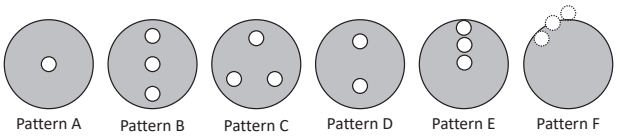

Fig. 9 Patterns using in order to assess detection ability of the US technique with non-deformable facility

and decreasing the time when the first echo is received by the US transducer. 50 % increase has been measured for 1 mm stainless steel ball compared to the maximum amplitude of the signal without any ball. Up to 10 mm ball, the magnitude of the shift peak echo increases 1000 %. Likewise, a similar trend has also been observed for the time delay. The first echo received by the US transducer has been shifted back around 1.4 % and 4 % for 1 mm ball and 2 mm ball respectively. 20 % change in time delay has been observed for 10 mm ball. Fig. 9 illustrates the comparison of all specimens examined. To sum up, the magnitude and time delay of the shift peak echo can be tracked to estimate the ball diameter underneath the US transducer.

Pattern B, C, D, and E investigate several balls in a specific arrangement for either single diameter or different diameters at the same time. According to the results, the magnitude and time delay of the shift peak echo completely depends on the highest specimen occupying on the bottom surface. In order to discriminate between different arrangements and ball sizes clearly, the US beam structure should thoroughly be defined beforehand.

Pattern F assesses the single ball for a specified diameter to investigate the effect of overlapping. Overlapping of the ball describes the conditions that are adjacent to the boundary, on the boundary, and out of the US beam. The result show that the ball can be detected even on the boundary except out of the US beam.

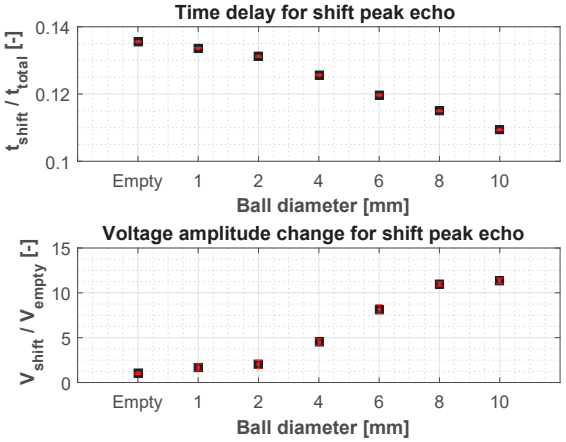

Fig. 10 Examination of time delay and amplitude change for shift peak echo for varying diameters using Pattern A

Since an exact conclusion about location & distribution of stainless steel ball underneath the US sensor has not been obtained from the pattern investigation, an additional experiment has purposefully been performed to extract the

US beam structure in terms of isoecho contour for a cross-sectional area underneath the US transducer on the bottom surface. In order to achieve this, a stainless steel ball has been placed for several region through 13 mm nominal element size of the US transducer. Experiments have been realized for 1 and 2 mm stainless steel balls separately in which a single ball is spontaneously spread through radial direction to extract the US beam structure. The location of the ball for each measurements is captured by an HD camera arranged below the experimental setup. The images are processed using Matlab image processing tool afterward. Figs. 11 and 12 show the change in the amplitude of the shift peak echo and surface peak echo respectively for each location assessed. All 1 mm and 2 mm balls have been detected which spread out through the US beam cross section. At least 10 % increase in the shift peak echo has been observed for both 1 and 2 mm balls compared to maximum signal for the same region where no bubble presents. In addition, 5 % difference in maximum has been observed for the surface peak echo

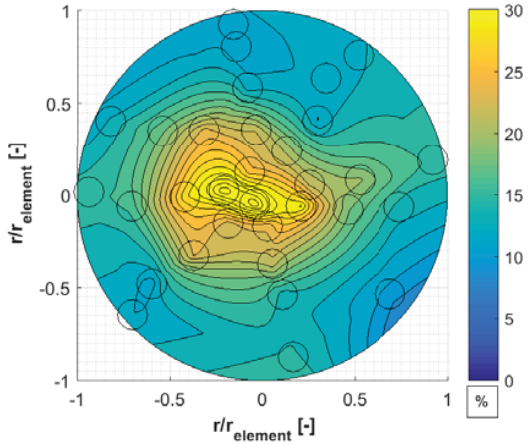

Fig. 11 Isoecho contour for percent change of the shift peak echo amplitude using 1 mm stainless steel ball

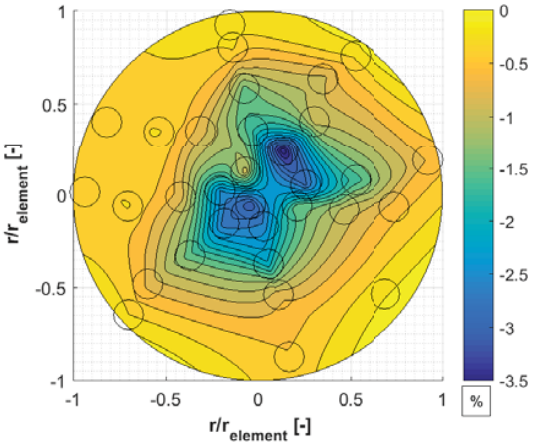

Fig. 12 Isoecho contour for percent change of the surface peak echo amplitude using 1 mm stainless steel ball

C. Air Injection

In order to get much more closer to simulate bubble formation experimentally, injection of air-bubbles inside a quiescent water seems an adequate method. Fig. 2 illustrates main differences between preliminary and secondary experimental setups promoting pulse-echo propagation through mediums. Yet the same US transducer and technique are applied for both setups, processing of data obtained from experiments diverge due to geometric singularities. The water temperature throughout experiments was measured 18° C.

1) Application of Couplant: An experimental study has been performed for several couplant thicknesses from direct contact to 4 mm distance between surfaces. Notably, direct contact means that after covering the front wall with the couplant, the US transducer is sunk into the gel until surfaces get as close as possible enabling a thin couplant layer. Having a direct contact between the US transducer and application surface greatly attenuates reflections coming through interface somewhat. Interpreting experimental results and foreseeing the danger of bubble occurrence inside the couplant, the thickness for application is sustained as the direct contact for the experiments conducted further.

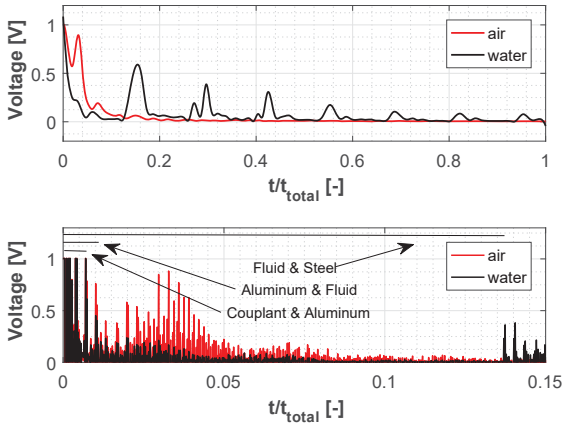

Fig. 13 Front wall reflection characteristics with and without water

2) Front Wall Effect: The bubble injection facility which has been designed based on real application encompasses several interfaces. Propagation of echoes through domain comes across with a characteristic signal between two adjacent pulses. In order to discover this characteristic, an experimental study based on the bubble injection facility has been prompted for the test case with and without water. The results investigating front wall effect are shown in Fig. 13. The effect of the front wall presence on signal characteristic profoundly affects the region where the shift peak echoes are obtainable.

3) Film Boiling: To simulate film boiling using the same experimental facility, an air clearance is kept which means the back surface of the tank is completely filled by air. Experimental study has been realized for the clearance with 2, 5, and 8 mm and compared to water-filled tank which is expressed in Fig. 14. Enabling a clearance on the upper side moves the surface peak echo back on the time domain since the total distance between the lower and upper part is decreased.

Compared to water-filled tank, the magnitude of surface peak voltage slightly increases due to higher reflection coefficient between the water-air interface than water-steel one.

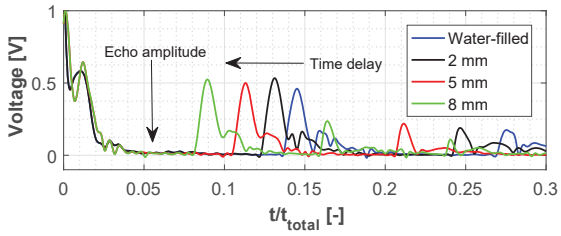

Fig. 14 Simulation of film regime simply keeping an air clearance between back wall and water surface

4) Bubble Injection: Four different apparatuses are designed having different arrangements for bubble injection process demonstrated in Fig. 15. Apparatus 1, which has no injection hole, is implemented to determine back echoes comes through in the case that no bubble being injected. Apparatus 2, 3 and 4 are set to explore the effect of bubble diameter and local arrangement.

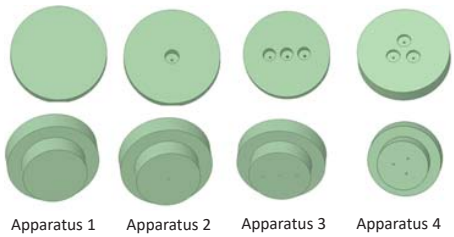

Fig. 15 Bubble injection apparatuses for air injection facility

The bubble diameter is controlled with a microliter syringe which precisely controls the amount of air injected. Likewise, an HD camera is set to take photographs during experiments to determine the bubble diameter within a common image-processing method later on. Experiments have been carried out for varying bubble diameters from 0.5 to 6 mm.

Fig. 16 shows the results for single bubble injection achieved by using apparatus 2. Due to the oscillations coming through the interface between the front wall and the others, the shift peak echo is completely attenuated especially for the bubbles 0.5 to 2 mm as can be seen in Fig. 16. On the other hand, since the continuous propagation of echoes among interfaces, an accumulation has been discovered while a bubble occupies inside the domain. This accumulations greatly increase as shown in Fig. 16 until the last echo completely attenuated before the adjacent pulse. In order to understand the effect of accumulation, 7 different windows encompassing echoes reflected back from the back wall have been examined taking RMS of each window separately to figure out accumulation compared to the signal acquired without bubble as a baseline. Fig. 17 demonstrates the accumulations for each window for a range of the bubble diameters. The accumulation characteristic of the first experimental setup is also shown in Fig. 17 using 1 and 2 mm stainless steel balls. The first

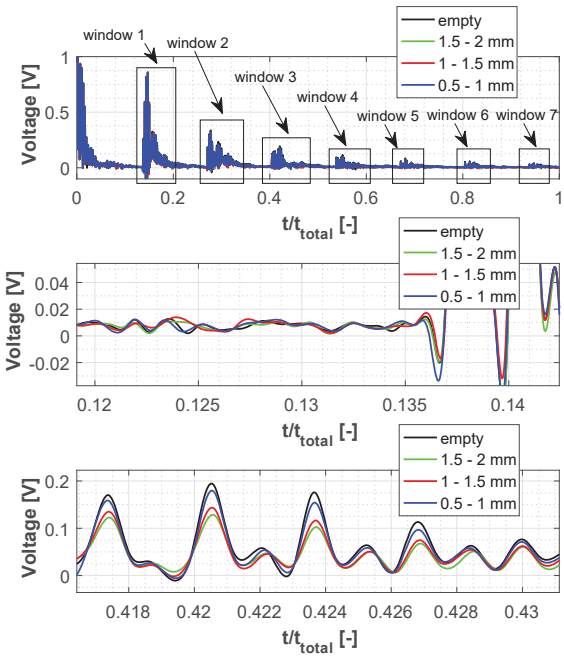

Fig. 16 Single bubble injection experiments applying apparatus 2

window has a relatively lower reduction due to the first pulse which is stronger than echoes oscillated afterward. A slight increase through windows has been obtained for all ranges of diameters. For the post-processing which has continuously been evaluated, the effect of the accumulation should definitely be taken into account.

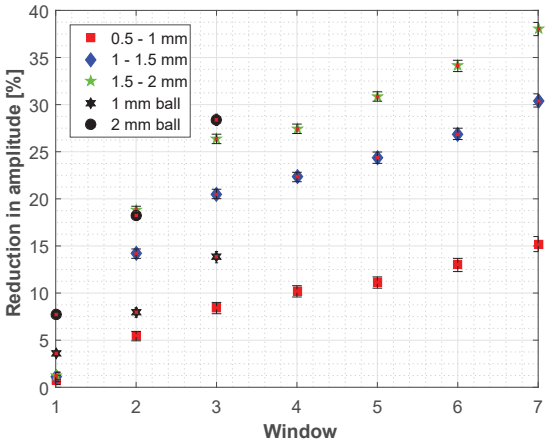

Fig. 17 Accumulation effect on the windows generated for Apparatus 2 (air injection) and Pattern A (steel ball)

IV. Detection Algorithm

A robust post-processing method has eventually been concluded which prevails over ambiguities arose. Instead of searching manually for the change of the echogram characteristic, a detection algorithm has preferably been developed which can run several cases concurrently so as to predict whether an irregular boundary is available underneath

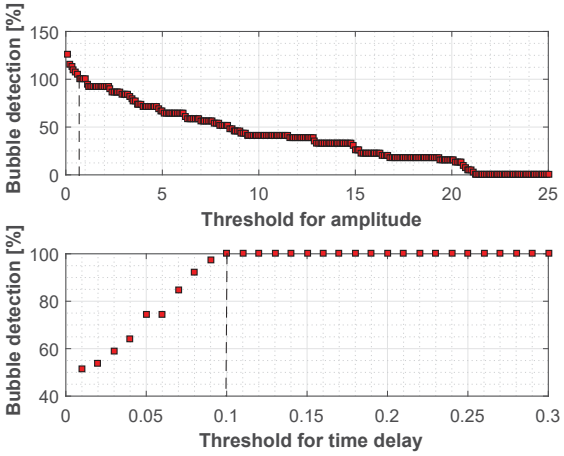

Fig. 18 The effect of thresholds for amplitude and time delay on bubble detection ability of the algorithm

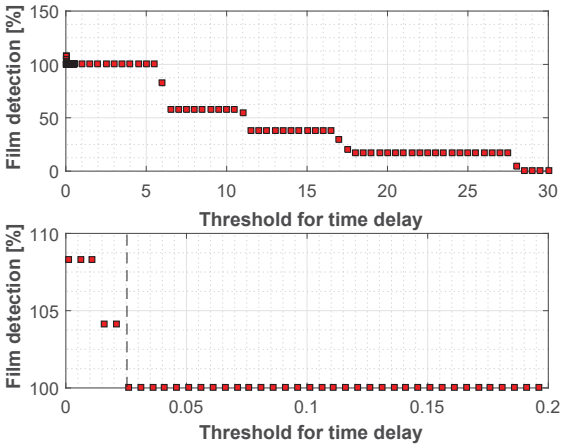

Fig. 19 The effect of threshold for time delay on film structure detection ability of the algorithm

the US transducer. The fundamental constraints concluded throughout experiments to determine detection algorithm can be summarized as follows.

Shift peak echo amplitude: Due to the interfaces between the US transducer and air bubble for the air injection facility, the shift echo peak is obscured drastically in an irretrievable way. The mere method to detect the shift echo peak in such systems is to increase both frequencies of the US transducer, and the distance between the US transducer and back surface where the bubbles are injected. Concerning dimensional constraints for the real application, it is not feasible to increase the distance. Therefore, the shift echo peak has been dismissed for the present detection algorithm.

Shift peak echo time delay: As it is mentioned for the shift echo peak, the same issue affects the shift echo time delay which disappears completely whilst performing an experiment with the bubble injection facility. The shift echo time delay has therefore been ignored for the detection algorithm as well.

Surface peak echo amplitude: One of the significant outcomes obtained within the echogram is the surface echo peak which is a straight reflection of pulse from the water & stainless steel back wall interface. A huge percentage of the pulse emitted into the domain is reflected by this interface due to being flat. The amplitude of the surface echo peak is related with the reflection coefficient of the interface and flatness of the surface where the pulse reflected back as an echo. According to experimental studies to understand the change in amplitude, the magnitude is gradually mitigated by increasing diameter of either steel ball or air bubble. Hence the magnitude of the surface echo peak can purposefully be processed to predict the diameter of the bubble. On the other hand, covering the back surface with an air layer such as film regime amplifies the surface peak echo amplitude because of the higher reflection coefficient of water & air interface than water & stainless steel one.

Surface peak echo time delay: Unless the back surface is covered with a layer such as a film regime, the surface echo would have emerged without any delay in time barring uncertainty. In order to shift surface echo back in the time domain, the back surface should almost be covered with a layer. Increasing the thickness of the layer results in shifting back in the time domain more.

RMS: As it is observed from experimental results, the characteristic of the signal has been altered by the bubble occupying inside the US beam underneath the back wall. This characteristic is transmitted into the whole signal after the surface echo peak received that causes incrementally reduction for the amplitude of the surface echo peak and all local peaks. Taking the RMS of the whole raw signal after the second surface echo peak which is detected by envelope, the post-processing method is greatly improved to distinguish phases.

Thresholds: In order to determine whether an acquired signal comprises an information for phase detection, several thresholds should be specified for the criteria explained beforehand to distinguish phases. The schematic illustration of the algorithm developed is shown in Fig. 20. A comprehensive study has been prompted in which thresholds for amplitude and time delay are purposefully anticipated. Examination has been carried out considering bubble injection and film structure as separate cases. Fig. 18 shows the trends of amplitude and time delay in regards to increasing threshold level for the single bubble injection using Apparatus 2. The bubble diameter varies between 0.5 to 2 mm for 40 different instantaneous measurements. Several measurements for the empty case at where no bubble presents have been conducted so as to enable comparison. 100 % detection means that all the bubbles injected into domain have been detected. In the case that the detection gets higher that 100 %, some empty cases have been counted as comprising bubble due to threshold which is defined inside uncertainty. The dashed lines are bound levels in which all the bubbles can be detected. Concerning bound levels, thresholds for amplitude and time delay have been set to 0.7 and 0.25 respectively.

In the case that a film structure presents underneath the US transducer, a certain time delay emerges which eases to distinguish phases. Detection of the film structure according to increasing level of the threshold is shown in Fig. 19. The air clearances examined during experiment varies between 1 to

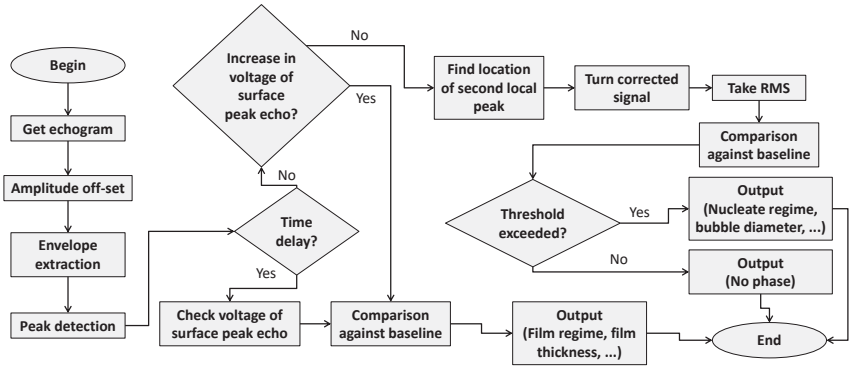

Fig. 20 Scheme of the final detection algorithm developed through the experimental studies

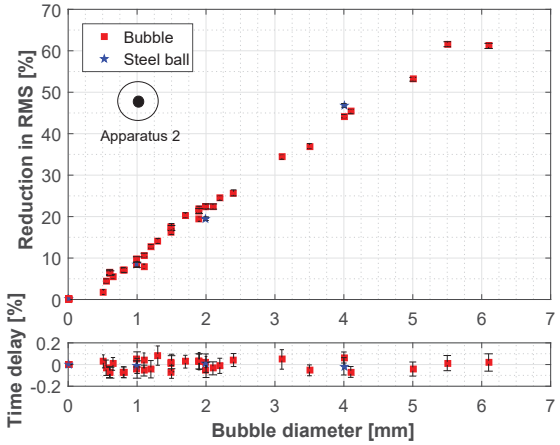

Fig. 21 Results for Apparatus 2 injecting bubble with various diameter to determined reduction in RSM and time delay

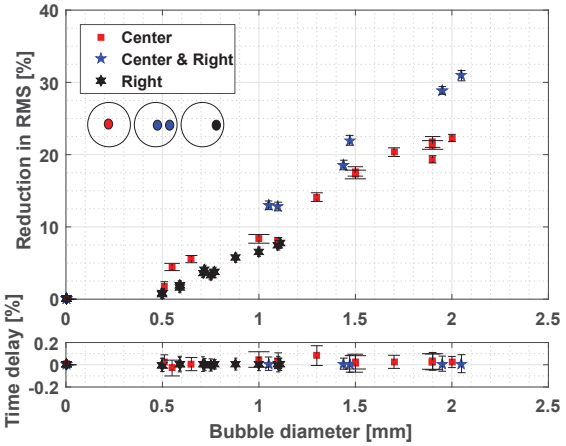

Fig. 23 Presence of the bubbles for different configurations underneath the US transducer to assess change in RMS and time delay

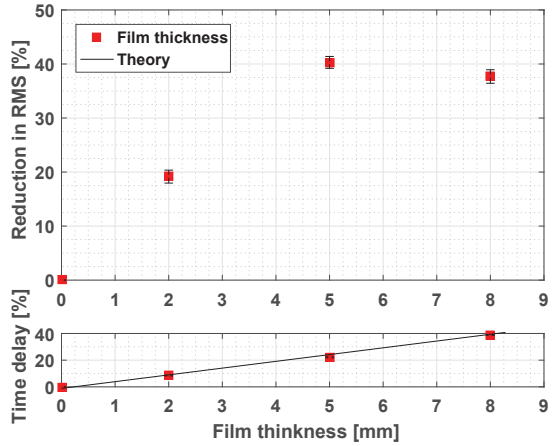

Fig. 22 Effect of the air clearance on reduction in RMS and time delay simulating film boiling inside partly water filled tank

10 mm. Implying a threshold bigger than 0.025, the detection rate for the film structure is obtained 100 % which is quite lower than the thresholds define for the bubble injection. Since the time delay provides enough information to distinguish film structure, the change in amplitude also gives some reasonable outcomes. At least 20 % increase has been obtained whilst the surface is covered with a film structure. To sum up, thresholds for amplitude and time delay have been determined as 0.7 and 0.25 respectively taking all the measurements and phases into account.

Using the algorithm being developed, the results for the bubble injection facility have been assessed based on reduction in RMS and time delay compared to baseline data in which no phase presents. In Fig. 21, a set of experiments has been delivered injecting bubble with various diameters to testify system characteristics. The results for 1, 2 and 4 mm stainless steel balls examined within the non-deformable body facility have also been implied.

Having been observed through experiments, increasing bubble diameter results in increasing reduction of RMS. Since the back wall surface is partly covered with a bubble, a time delay would not be expected whereas a high percentage of the pulse is reflected by the back wall still. Time delay which spreads out increasing the bubble diameter varies between ± 0.2 %. For 1 mm bubble, the reduction in RMS is close to 10 % which is quite compatible to detect individually.

Aside from the bubble occurrence, the effect of the film simulated with air clearance kept between back wall and water surface has been investigated as shown in Fig. 22. The main outcome of the film boiling is time delay that can be calculated

implying the theory explained beforehand. According to experimental results, time delay increases linearly through ascending film thickness. A considerable reduction of RMS has also been noticed. Further, an increase in the amplitude of the surface peak echo has been observed due to the fact that the reflection coefficient of water & air interface is higher than water & steel interface.

Being extracted isoecho contours for a cross-sectional area of the US beam using steel balls, an experimental study has also been concluded as to discuss spatial distribution of air-bubbles. In Fig. 23, assessment on three different arrangements has altogether been shown. Compared to center positioning, presenting a bubble on the right side lowers detectability around 1.5% which has also been determined within isoecho contour expressed in Fig. 11. Having two separate bubbles for both right and center positions on the same apparatus has partially been detected easily due to covering the back wall for a higher percentage than single bubble on the center. According to the algorithm developed based on experiments conducted so far, the phases during the boiling process can be distinguished as no boiling, nucleate boiling and film boiling which has been one of the main aims of the present project.

V. Conclusion

The US technique was broadly investigated and applied to understand, improve, and optimize boiling in engine cooling channels for space applications within an exploratory research campaign. The main aim of the project is to develop a preliminary detection algorithm to distinguish different phases during boiling process, and thereby keeping boiling process into nucleation site where the maximum heat flux may be reached for an efficient cooling cycle. Since the detection ability and applicability of the method were examined through experiments, a detection algorithm was developed which basically enables an affirmative solution to distinguish nucleate and film regimes into the fully opaque tank based on the accumulation of echoes through propagation. It is worth to mention that no study has been found in the literature using a similar method.

VI. Recommendations for Future Work

Given the above arguments about the US technique, carrying out a set of experiments is strongly encouraged to improve understanding of the method and detection algorithm. A further experimental study based on a vertical arrangement of the bubble injection facility would be quintessential to explore the applicability of the US technique for convective conditions in which the bubble moves upward. Additionally, an experimental study using either water or HFE-7000 would definitely be an appropriate way to determine boiling characteristics which is an important asset to improve and advocate detection algorithm.

References

[1] L. Olh, *Manual of Neurosonology: 1 - Ultrasound principles*. Cambridge University Press, 2016.

[2] M. Luque de Castro and F. Capote, *Analytical Applications of Ultrasound: Techniques and Instrumentation in Analytical Chemistry: Volume 26*. Elsevier Science, 2006.

[3] T. Richter, K. Eckert, X. Yang, and S. Odenbach, "Measuring the diameter of rising gas bubbles by means of the ultrasound transit time technique," *Nuclear Engineering and Design*, vol. 291, pp. 64–70, 2015.

[4] T. Nguyen, H. Kikura, H. Murakawa, and N. Tsuzuki, "Measurement of bubbly two-phase flow in vertical pipe using multiwave ultrasonic pulsed doppler method and wire mesh tomography," *The Fourth International Symposium on Innovative Nuclear Energy Systems, INES-4*, vol. 71, pp. 337–351, 2015.

[5] M. Hussein, W.and Khan, J. Zamorano, F. Espic, and N. Yoma, "A novel ultrasound based technique for classifying gas bubble sizes in liquids," *Measurement Science and Technology*, vol. 25, pp. 1–11, 2014.

[6] L. Kinsler, A. Frey, A. Coppens, and J. Sanders, *Fundamentals of Acoustics: Reflection and Transmission, 4th Edition*. John Wiley & Sons, 2000.

[7] J. Yoo, "Data sheet of olympus for the immersed us transducer," *Idaho National Laboratory*, 2016.

[8] F. Randall and F. Gregory, *Cryogenic Heat Transfer, Second Edition*. CRC Press Taylor and Francis Group, 2016.

[9] I. Pioro, W. Rohsenow, and S. Doerffer, "Nucleate pool-boiling heat transfer: Review of parametric effects of boiling surface," *International Journal of Heat and Mass Transfer*, vol. 47, pp. 5033–5044, 2004.

[10] A. Molina, "Experimental study of boiling in water and liquid nitrogen," *The von Karman Institute for Fluid Dynamics - Reseach Master Project Report*, 2014.

[11] W. Lei, Z. Kang, X. Fushou, M. Yuan, and L. Yanzhong, "Prediction of pool boiling heat transfer for hydrogen in microgravity," *International Journal of Heat and Mass Transfer*, vol. 94, pp. 465–473, 2016.

[12] M. Kida, Y. Kikuchci, O. Takahashi, and I. Michiyosh, "Pool-boiling heat transfer in liquid nitrogen," *Journal of Nuclear Science and Technology*, 1980.

[13] X. Zhang, J. Chen, W. Xiong, and T. Jin, "Visualization study of nucleate pool boiling of liquid nitrogen with quasi-steady heat input," *Cryogenics*, vol. 72, pp. 14–21, 2015.

[14] J. Yoo, "Bubble departure diameter and bubble release frequency measurement from tamu subcooled flow boiling experiment," *Idaho National Laboratory*, 2016.

[15] J. Yoo, C. Estrada-Perez, and Y. Hassan, "Experimental study on bubble dynamics and wall heat transfer arising from a single nucleation site at subcooled flow boiling conditions part 1: Experimental methods and data quality verification," *International Journal of Multiphase Flow*, vol. 84, pp. 315–324, 2016.